Chapter 8

ENHANCEMENT OF THERMOELECTRIC PERFORMANCE IN SrTiO₃-BASED CERAMICS BY PROCESSING CONDITIONS

Alexander Tkach[1,], João Resende[1],*
Pablo Diaz Chao[2], Emmanuel Guilmeau[2],
M. Elisabete Costa[1] and Paula M. Vilarinho[1]

[1]CICECO – Aveiro Institute of Materials, Department of Materials and Ceramic Engineering, University of Aveiro, Aveiro, Portugal

[2]Laboratoire CRISMAT, CNRS, ENSICAEN, Caen, France

ABSTRACT

Currently much worldwide research is focused on clean and sustainable energy sources that can respond to the rising energy demands of the world. Thermoelectric (TE) harvesting of unused heat in automotive exhaustion, industrial processes and home heating will increase the

---

[*] Corresponding Author's E-mail: atkach@ua.pt.

efficiency of energy use, while simultaneously reducing the CO_2 emissions.

Although a number of high TE performance materials, such as Te-based, Se-based and intermetallic compounds, have been developed so far, most of them suffer from toxicity, mineral scarcity and high cost, which are problems for universal application. Moreover, they are limited in their ability to harvest electricity from solar, automotive and industrial waste heat, due to their decomposition and volatilisation at elevated temperatures. As a result, new, nontoxic, more stable, naturally abundant, light-weight and low-cost materials based on oxides have to be developed, despite the fact that oxides are of low carrier mobility and high thermal conductivity in general. Thus, p-type oxides based on cobaltates have been found to be very promising, especially in high temperature ranges. To date, n-type oxides with equivalent TE performance have yet to be discovered to produce effective p-n TE modules.

Here we will summarise the most relevant studies devoted to the TE behaviour of n-type $SrTiO_3$-based ceramics. Doping, nonstoichiometry and other important parameters to enhance the TE performance will be discussed. Particle size of Nb-doped $SrTiO_3$ powders, together with sintering conditions, will also be shown as key parameters able to increase the TE figure of merit, either by microstructure engineering or by densification.

Keywords: perovskite oxide electroceramics, donor doping, sub-micrometre particles, two-step sintering, microstructure engineering, thermoelectric figure of merit

INTRODUCTION

Global Problem

Efficient technologies to harvest energy are becoming crucially important in this century. The world's population, numbering today some 7.7 billion people, may approach 11.8 billion by the year 2100. As the population doubled, the global energy supply tripled. Currently, fossil fuels provide around 66% of the world's electrical power, and 95% of the world's total energy demand including heating, transportation, electricity generation and other uses. However, the burning of fossil fuels releases CO_2, being thus

the largest contributing source of greenhouse gases and greenhouse effect, and as a consequence, of global warming.

Transport makes a significant contribution to overall emissions of CO_2, creating around 26% of the total CO_2 emissions in Europe, with cars producing ~12%. Limited by regulation, in 2009 CO_2 emissions equalled an average of 130 g of CO_2/km. From 2020, this level is to be reduced to 95 g of CO_2/km. In addition, only a small portion (around 25%) of the energy supplied by the fuel is used in the propulsion of the vehicle, the rest being lost essentially in exhaust heat, unburnt fuel and friction [1]. The annual waste heat generated by automobiles is estimated at 45.8 Tcal, and virtually all of this waste heat is discharged from engines using fossil fuels. Therefore, in the automotive sector the use of thermoelectric (TE) generators driven by waste heat at both radiator and exhaust gas systems could increase the fuel efficiency by up to 5% or even more, depending on the size of the vehicle and the TE technology used.

Furthermore, with the advent of hybrid vehicles, TE is becoming a key technology. Most of the automobile companies are introducing hybrid vehicles, which have two or more distinct power sources for moving the car: an internal combustion engine and one or more electric motors. The engine is separated from the direct powertrain via electrical power lines that require efficient energy recovery and storage, in which TE devices are particularly useful. The TE device acts as additional energy source for battery charging. Hybrid vehicles will have low fuel consumption and increased efficiency with low CO_2 emissions and low environmental impact.

State of the Art

As discussed above, TE technology is quite promising for scavenging the energy available in the exhaust heat, combining furthermore some additional advantages as no moving parts, no noise and an exceptional reliability. The TE effect is the direct conversion of temperature difference into electrical power and vice versa. Direct effect occurs when electricity

appears between cold and hot parts of the TE materials [2], and its efficiency is related to the dimensionless figure of merit of the TE material *ZT*:

$$ZT = S^2 \times \sigma \times T / \kappa \qquad (1)$$

where *S*, *σ*, *T*, and *κ* stand for Seebeck coefficient, electrical conductivity, absolute temperature and thermal conductivity, respectively [3]. Thus, the ideal TE material is characterised by high electrical conductivity and Seebeck coefficient together with low thermal conductivity. Indeed, it should behave as a "phonon-glass electron-crystal" (PGEC), i.e., have a lattice *κ* as low as that of a glass (typically of the order of 10^{-3} W/(K·cm)) [4], and *σ* as high as that of crystals (around 10^3 S/cm) [5, 6]. Semiconductor TE materials are classified as n- and p-type, with electrons and holes, respectively, serving as the main charge carriers. Both n- and p-type materials, being connected electrically in series and thermally in parallel, are required for a TE module [4].

TE technology has been available for a long period; however, the current TE materials with the highest figure of merit, *ZT* > 1 are Te-based, Se-based and intermetallic compounds, most of which are toxic, rare and of high cost, being these attributes undesired barriers to TE universal applications, particularly in what the environmental impact is concerned [7]. Furthermore, they are limited in their ability to harvest electricity at temperatures above 300ºC, such as that of vehicle exhaust gas [8], or solar and industrial waste heat, due to their decomposition and volatilisation at elevated temperatures [7]. As a result, there is a need to develop new, nontoxic, more stable, naturally abundant, light-weight and low-cost materials based on oxides, despite the fact that oxides exhibit in general low carrier mobility and high thermal conductivity. The representative p-type materials with *ZT* up to 1 are $NaCo_2O_4$, $Ca_3Co_4O_9$ and $Bi_2Sr_2Co_2O_y$, which have been found very promising especially in higher temperature ranges, benefiting from their layered structure [9-11]. The best *ZT* reported until now is ~1.2 for p-type single crystal $Ba_2Sr_2Co_2O_y$ whiskers [11]. To date, n-type oxides with equivalent *ZT* values are yet to be discovered to not restrict the efficiency of the p-n TE module, although it is extremely difficult to

increase the performance to *ZT* > 1 because electrical and thermal conductivities are properties displaying mutual dependence [3].

The most promising candidates for n-type TE oxides include ZnO, $CaMnO_3$ and $SrTiO_3$ (STO) with suitable doping [3]. Possessing a typical perovskite ABO_3 structure with Sr^{2+} ions at the cube corners (A site), Ti^{4+} ions occupying the cube centre (B site), and O^{2-} ions at the cube faces, as shown in Figure 1, STO is an intrinsic insulator with bandgap of 3.2 eV [3] and high dielectric permittivity. Moreover, its permittivity and, hence, capacitance can be strongly enhanced by donor doping [12-14], making this material useful for high-voltage capacitor applications [15], despite the fact that this effect is extrinsic, since such doping stiffens the transverse optic TO1 mode [16]. On the other hand, the electrical conductivity can be increased in STO, thus enhancing its TE performance by the so-called donor-doping with higher valence ions on the A- or B-site, and by reduction leading to oxygen vacancies [17-33].
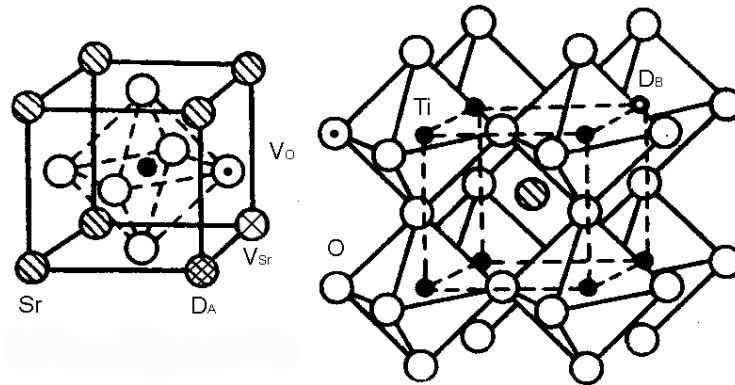

Figure 1. Cubic perovskite crystal structure of $SrTiO_3$-based materials with strontium ions marked as Sr, titanium ions marked as Ti, oxygen ions marked as O, A-site donor ions marked as D_A, B-site donor ions marked as D_B, strontium vacancies marked as V_{Sr} and oxygen vacancies marked as V_O.

Regardless the fact that the first report on the TE performance of reduced bulk STO appeared in 1964 [17], it has attracted tremendous interest as an n-type TE oxide only at 2000th, due to its large carrier effective mass, stability at high temperature and structural tolerance with respect to

doping [18]. A *ZT* value of ~0.1 was reported for $Sr_{1-1.5x}La_xTiO_3$ single crystals with x ≤ 0.1 in 2001 [19]. As a result of a substantially high σ and a large *S*, the power factor $S^2\sigma = 2.8\text{-}3.6$ mW/(K^{2}m) obtained in STO heavily doped by rare earth ions on the Sr site, as well as by Nb or Ta on the Ti site, was found to be comparable to that of conventional TE materials [19]. However, due to the relatively high κ [20], the highest *ZT* values which could be obtained by single site doping in STO, are only in the order of 0.35-0.41 at temperatures of 970-1100 K [20-22, 25, 30, 33], as shown in Figure 2. In 2006 Ohta et al. reported a *ZT* value of 0.35 at 1000 K for ~20-µm-grain-size $SrTi_{0.80}Nb_{0.20}O_{3\pm\delta}$ ceramics hot pressed at 36 MPa and 1400°C for 2 h in an Ar atmosphere, although on cooling toward room temperature *ZT* diminished below 0.01 [20]. Then, in 2010 Kikuchi et al. prepared $Sr_{0.92}La_{0.08}TiO_{3\pm\delta}$ ceramics by combustion synthesis with post-spark plasma sintering at 1300°C, finding that the 5-min-sintered ceramics recorded the largest figure of merit of 0.37 at 1045 K [21], as also presented in Figure 2. In 2014, the same value was obtained by Park et al. in $Sr_{0.91}La_{0.09}TiO_{3\pm\delta}$ but at 973 K [22], while Dehkordi et al. could measure a *ZT* of 0.35 in $Sr_{0.85}Pr_{0.15}TiO_{3\pm\delta}$ at only 773 K [23], using spark plasma sintering (SPS) at 1400-1500°C for 5 min. The later results were explained by incomplete solid solubility of Pr in STO, and thereby Pr-rich grain boundaries [24].

As also shown in Figure 2, in 2014 Kovalevsky et al. reported that among STO ceramics doped with 10 at.% of trivalent ions at the Sr site, conventionally sintered in air at 1700°C for 10 h and further reduced in a $10\%H_2\text{-}90\%N_2$ atmosphere at 1500°C for 10 h, the $Sr_{0.90}Dy_{0.10}TiO_{3\pm\delta}$ composition reveals the highest *ZT* value of 0.41 at 1073 K and 0.42 around 1200 K [25]. The following year, Yaremchenko et al. displayed that identically prepared Ta-doped STO ceramics can yield TE performance comparable to that of Nb-doped STO, particularly in case of the Sr deficient composition $Sr_{0.95}Ti_{0.90}Ta_{0.10}O_{3\pm\delta}$, yielding the figure of merit values of 0.3 at 1000 K and 0.37 at 1230 K [28]. Moreover, there were several reports on the fact that the electrical conductivity of donor-doped $SrTiO_3$ is sensitive to Sr content, and that the Sr deficient compositions sintered in reduced atmospheres have a much higher electrical conductivity, thereby enhancing TE performance compared to their stoichiometric counterparts [26-28, 30,

34]. Thus, as indicated in Figure 2 as well, the highest *ZT* value for single site doped STO was reported by Lu et al. to reach 0.41 at 973 K in the case of $Sr_{1-1.5x}La_xTiO_{3\pm\delta}$ ceramics with $x = 0.15$, conventionally sintered in a flowing $5\%H_2-95\%N_2$ gas at 1500°C for 6 h and then cooled at 30°C/min [30]. Furthermore, in 2015 Zhang et al. reported that TE performance of Nb-doped STO can be improved up to a *ZT* of 0.4 at 1100 K for $SrTi_{0.90}Nb_{0.10}O_{3\pm\delta}$ ceramics [29], using the hydrothermal method for nano-powder fabrication, and muffle furnace sintering at 1300°C for 5 h within a bed of carbon powder. Finally, using the same preparation method, the record *ZT* values of 0.6 at 1000 K and 0.65 at 1100 K were reported by Wang et al. for double site doped $Sr_{0.90}La_{0.10}Ti_{0.90}Nb_{0.10}O_{3\pm\delta}$ ceramics in 2017 [32].
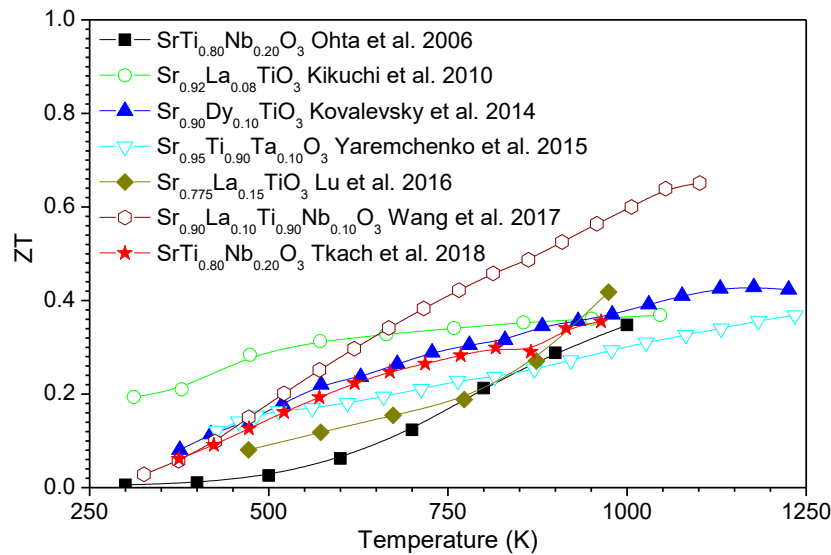

Figure 2. Dimensionless figure of merit (*ZT*) values of $SrTiO_3$-based ceramics as a function of temperature.

As Figure 2 shows as well, we have recently reported that $SrTi_{0.80}Nb_{0.20}O_{3\pm\delta}$ ceramics, conventionally sintered in air at 1450°C and further in $10\%H_2-90\%N_2$ at 1400°C, can reveal *ZT* values up to 0.36 at 970 K [33]. Such values are observed only when the ceramics were prepared from centrifuged powders having an average particle size of 270 nm, while

for the ceramics prepared from powders with 800 nm average particle size ZT just reached 0.14 at 970 K. Corresponding enhancement of the TE performance was explained as a result of a bimodal grain size distribution due to abnormal grain growth (AGG) [33].

On the other hand, the room-temperature figure of merit of 0.42 was reported for $Sr_{0.900}La_{0.067}TiO_{3\pm\delta}$ ceramics modified by addition of 0.6 wt.% of reduced graphene oxide (rGO) sheets, whereas *ZT* at 1023 K was increased from 0.12 for monophasic ceramics to 0.36 for those with graphene nano-inclusions [35], although rGO itself is not the best TE material [36]. These results are in agreement with reports on enhanced *ZT* values of Nb-doped STO by nano-inclusions of yttria stabilised zirconia [37], and those of La and Nb co-doped STO with Cu or Fe metallic nano-inclusions [38], as well as with the figure of merit of Nb-doped and undoped STO being raised with addition of rGO [34, 39].

Thus, according to the literature review, different approaches can be considered to improve the TE performance of oxide materials: (i) creating lattice defects like O and Sr vacancies [26-28, 30, 31, 34], (ii) grain boundary engineering involving nano-inclusions [23, 24, 34, 35, 37-39] and (iii) grain nano-structuring using nano-powders [21, 22, 29, 32].

The first approach behind enhanced conductivity involves phonon scattering within the unit cell by creating point defects such as vacancies. Complex crystal structures can be used to separate the electron-crystal from the phonon glass. Here the goal is to achieve a phonon glass without disrupting the crystallinity of the electron-transport region. Moreover, in contrast to the previous assumptions that the Ruddlesden–Popper (RP) structure, forming at the regions of Sr excess, can help to improve the TE performance of STO-based materials [3], Sr deficiency was found to be more effective in enhancing *ZT* [26-28, 30, 31, 34].

The second approach lies in the phonon scattering at interfaces, via the use of multiphase composites mixed at the nanometre scale [23, 24, 37] and to suppress the grain boundary resistivity as in the case of metallic and graphene-derived nano-inclusions [34, 35, 38, 39].

The third approach involves the decrease of the grain size, so that approaching quantum confinement results in the disruption of the phonon

paths, contributing to a decrease of the thermal diffusivity of the material [21, 22, 29, 32]. Indeed, reducing the grain size and nano-structuring has been theoretically reported to lower the value of the thermal conductivity [40]. An increase in the number of such interfaces, as grain boundaries, will increase the phonon scattering in the polycrystalline structure, leading to a decrease of κ [3]. Additionally, the reduction of the grain size will increase the scattering of the phonons with shorter mean free paths at the grain boundaries, creating a wider range of scattered phonons [3].

The later approach, however, is problematic, since reducing the grain size leads to an increase in the electrical resistivity, which is not favourable for enhancing the *ZT* values [41]. To overcome such dual effect of grain size, high-performance TE ceramics may need to be a combination of coarse and fine grains in an individual material, as was shown by us on the example of the $SrTi_{0.80}Nb_{0.20}O_{3\pm\delta}$ ceramics [33]. Then, the coarse grains can afford high electrical conductivity to the ceramics, while their thermal conductivity may be reduced by the enhanced scattering effect in the fine grains and their boundaries, because phonons do not "select" their path like electronic carriers. Within this context, we have proposed the use of AGG to obtain the required bimodal grain size distribution in STO based oxide ceramics for the optimisation of the TE figure of merit [33].

Indeed, bimodal grain size distribution in ceramics is usually related to AGG, whereas the temperature range where AGG occurs depends on the initial powder average particle size, as was observed in STO ceramics with an addition of 0.5 at.% of Nb [42, 43]. In these ceramics prepared from 3-μm-size powders, AGG started at 1500°C and was completed at 1540°C. In STO ceramics prepared with 500-nm size powders, the onset and completion temperatures of AGG decreased to 1460 and 1510°C, respectively. Finally, for 300-nm-size powders, the AGG temperatures decreased further to 1445 and 1470°C, respectively [42, 43]. Following this trend, and using a Nb_2O_5 precursor with higher purity (99.9%) as compared to that of $SrCO_3$ (99%) and TiO_2 (99%), a ~0.2 at.% excess of B-site ions is anticipated in $SrTi_{0.80}Nb_{0.20}O_{3\pm\delta}$. This excess is expected to favour the formation of a liquid phase and, thereby, to promote the AGG in the ceramics prepared from powders with a fine particle size of 270 nm on average, and sintered at 1400-

1450°C [33]. For that, Nb-doped STO powders were prepared by conventional mixed oxide method and separated into coarse and fine particle size powders by centrifugation. Then, similar to the fabrication of $BaTiO_3$ with mm-scale grains [44], a two-step firing, consisting of sintering in air at 1450°C for AGG nucleation in fine-size powder ceramics, and further firing at 1400°C for the growth of selected grains, was carried out [33].

Thus, observing that the microstructural tuning of 20 at.% Nb-doped STO by starting powder morphology and sintering cycle design in conventionally sintered ceramics can result in an increase of *ZT* values from 0.14 to 0.36 at 970 K [33], we have decided to study whether it is applicable for ceramics with other doping levels. Since there are already many reports on STO with Nb content between 10 and 20 at.% [20, 26, 29, 31-34, 37], which is thought to be optimum for enhanced TE performance, we have chosen only 5 at.% Nb doping of STO for this study, which was reported so far only by Zhang et al. [29] to our knowledge.

METHODS

Preparation

Preparation of 5 at.% Nb-doped STO ceramics was divided into three main parts: powder preparation, adjustment of the particle size and two-step sintering processes. These preparation steps affect the ceramics' densities and grain size distribution. $SrTi_{0.95}Nb_{0.05}O_{3\pm\delta}$ (STN5) ceramic compositions were prepared by a solid-state reaction of mixed powders of $SrCO_3$ (Merck, 99%), TiO_2 (Sigma-Aldrich, 99%) and Nb_2O_5 (Alfa Aesar, 99.9%) with the accurate stoichiometry. The powders were mixed by ball milling in Teflon jars at 300 rpm for 5 h with zirconia balls in an ethanol medium. The calcination was performed for 2 h at 1200°C with heating and cooling rates of 10°C/min. The powders were re-milled at 300 rpm for 72 h in ethanol. Coulter Multisizer (LS230, Beckman Coulter, Inc.) analysis revealed a double peak distribution of the powders' particle size after milling. For particle size separation, the powders were suspended in water with a

concentration of 20 g/L, stirred by ultrasound for 5 min, and centrifuged for 1 min at 1000 rpm. The supernatant slurry and the sediment were collected separately, filtered and dried in order to obtain fine (~320 nm on average) and coarse (~760 nm on average) particle powders, respectively. Circular section pellets of 10 mm in diameter and rectangular section pellets of 15 mm × 5 mm of each of these two powders were uniaxially pressed at 20 kPa for 30 s, followed by cold isostatic pressing at 200 MPa for 15 min. A two-step firing was used to sinter the ceramics. The pellets were sintered in air at 1450ºC for 10 h, and further in a 10%H_2-90%N_2 reducing atmosphere at 1400ºC for 10 h with heating and cooling rates of 10ºC/min.

Characterisation

Structural and microstructural characterisation was carried-out by X-ray diffraction (XRD), scanning electron microscopy (SEM) and optical microscopy. The room-temperature XRD analysis (Rigaku D/Max-B, Cu Kα) was conducted on the ground sintered ceramics. The diffraction angle (2θ) was in the range of 20-80º with a sampling step of 0.02º. The lattice parameter was calculated by a least-squares-approach fitting of the XRD data, using Rietveld refinement FullProf software. The microstructure of the ceramics was observed on polished and thermally etched sections, using SEM (Hitachi S-4100) and field emission SEM (Hitachi SU-70). The grain size distribution of the ceramics was obtained using the Feret diameter determination method within the image analysis software ImageJ. The electrical resistance and Seebeck coefficient were measured on a commercial ZEM 3 device (ULVAC-RIKO) in a partial helium atmosphere. The thermal conductivity was calculated from the specific heat capacity (C_p), density (ρ) and thermal diffusivity (α), according to the expression $\kappa = C_p \times \rho \times \alpha$. The thermal diffusivity was measured using a Laser Flash technique (NETZSCH LFA 457 MicroFlash), while the specific heat was calculated using the Dulong-Petit law as $C_p = 3N \times R/M$, where N is the number of moles including all atoms, R is the gas constant (8.314 J/(mol·K)) and M is the molar mass of the compound (g/mol) [45]. The estimated

measurement uncertainties are 6% for the Seebeck coefficient, 8% for the electrical resistivity, 11% for the thermal conductivity and 16% for the final figure of merit, *ZT* [46].

RESULTS

The density of the two-step-sintered 5 at.% Nb-doped STO ceramics is estimated to be 4.62 g/cm^3 and 4.91 g/cm^3 for ceramics prepared from coarse and fine particle size powders, respectively. The XRD profile of the ceramics shown in Figure 3 in a logarithmic scale reveals no distinct second phases. The observed X-ray diffraction lines are analogous for STN5 ceramics prepared from fine and coarse particle size powders, being also consistent with the cubic crystallographic structure of undoped STO (JCPDS #35-0734).

Using the lattice parameter 391.32(3) pm refined from this XRD profile and the molar mass for $SrTi_{0.95}Nb_{0.05}O_3$ composition of 185.77 g/mol, the theoretical density was determined as 5.14 g/cm^3. Therefore, the relative density of 5 at.% Nb-doped STO ceramics is <90% for coarse particle and >95% for fine particle size ceramics.
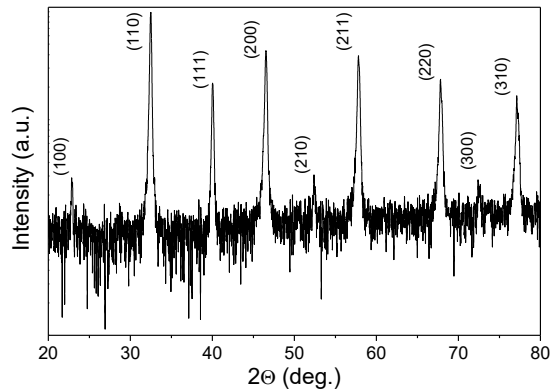

Figure 3. XRD profiles of STN5 ceramics sintered in air at 1450ºC for 10 h and further in H_2/N_2 at 1400ºC for 10 h, presenting reflections of $SrTiO_3$ phase marked by the corresponding indexes.
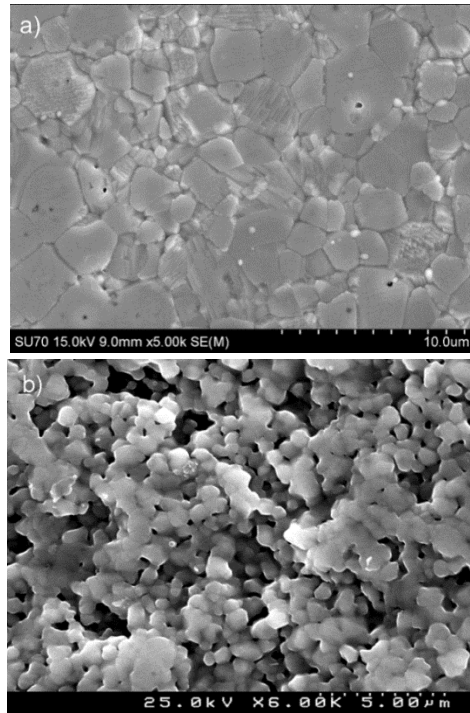
Figure 4. SEM micrographs of STN5 ceramics sintered from fine (a) and coarse (b) particle size powders at 1450ºC for 10 h in air and further at 1400ºC for 10 h in H_2/N_2, showing dissimilar microstructures.

The SEM micrographs of STN5 ceramics prepared from fine and coarse particle size precursor powders are shown in Figures 4a and 4b, respectively. These ceramics undoubtedly present different microstructures, according to the different density values. The average grain size for the ceramics prepared from coarse particle size powders is 1.1 µm, indicating that neither complete densification nor significant grain growth occurs in this case. On the other hand, for the chosen sintering conditions, fine-size powder yields STN5 ceramics with a twice-as-large average grain size of 2.2 µm, besides almost full densification.

The AGG trend formerly observed in STO ceramics with addition of 0.5 at.% excess of Nb [42, 43] is not verified here for STN5 ceramics. The grain growth was observed in fine-size powder ceramics during the sintering in air at 1450°C and further in H_2/N_2 at 1400°C, but it was not an AGG, since

grains larger than 2.5 times the average value were not found. The reason behind this observation can be related with the fact that the B-site ion excess derived from the higher purity of the used Nb precursor may not be sufficient to promote the AGG. Bae et al. used 0.5 at.% excess [42, 43], while in our previous work on $SrTi_{0.80}Nb_{0.20}O_{3\pm\delta}$ ceramics, about 0.2 at.% excess of B-site ions was expected due to the higher purity of the Nb precursor [33]. In the current work, however, no B-site ions excess was intentionally introduced, while the higher purity of the Nb precursor should only lead to ~0.05 at.% excess, which seems to be too low to promote the AGG.

On the other hand, for the coarse-size STN5 ceramics, the used firing conditions were not enough to densify the ceramics till high densities and, consequently to promote the grain growth. Therefore, the grains remained rather small. Despite these microstructure characteristics, we have evaluated the TE properties (electrical conductivity, Seebeck coefficient and thermal conductivity) of 5 at.% Nb-doped STO ceramics, since the presence of a high porosity decreasing the electrical conductivity may also decrease the thermal conductivity [47, 48]. Moreover, TE materials with a relative density down to 63.1% (including Nb-doped STO ceramics with *ZT* of 0.02 at 900 K [48]) were reported to show TE figure of merit up to 1.63 at 615 K [47].

The temperature dependence of the electrical conductivity (σ) of the STN5 ceramics is shown in Figure 5. The initial increase of conduction with temperature resembles that observed in electrical conductivity or charge carrier mobility for $SrTi_{0.8}Nb_{0.2}O_{3\pm\delta}$ fine grain ceramics [29] and polycrystalline films [20], but not for coarse grain ceramics or epitaxial films of the same composition [20]. The reduced carrier mobility at low temperatures was attributed to the structural distortion induced localised states originating from doping, and accelerated by the crystal size reduction [22, 29]. In agreement with this explanation, the peak temperature in Figure 5 increases with decreasing density and grain size for $SrTi_{0.95}Nb_{0.05}O_{3\pm\delta}$ ceramics. Moreover, the semiconductor-like increase of the conductivity until the peak temperature suggests that the localised electrons can be thermally excited [29]. A decreasing trend, indicating that phonon scattering becomes the dominant mechanism, is observed at high temperatures [20,

22]. The highest value of electrical conductivity is 106 S/cm at 525 K, which is about one order higher than 9 S/cm at peak temperature of 667 K for ceramics produced with coarser powders, and about twice as high as the value obtained by Zhang et al. with an identical composition [29].
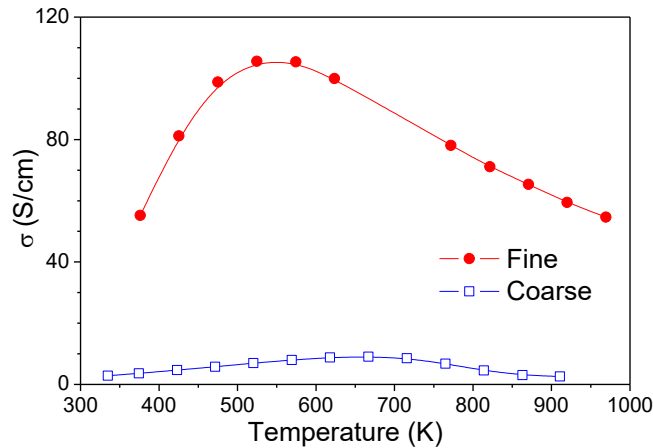

Figure 5. Electrical conductivity σ of STN5 ceramics produced from coarse (open squares) and fine (solid circles) particle size powders versus temperature, showing about one order difference for two ceramics.

Figure 6 shows the temperature dependence of Seebeck coefficient (*S*). *S* has negative values, confirming that both STN5 ceramics are *n*-type materials. The absolute *S* values of both ceramics increase with temperature, while displaying almost parallel trends. Ceramics produced with finer powders present more negative values of *S*, although the difference between the ceramics prepared from the two different precursor powders does not exceed 13%. The magnitude of the Seebeck coefficient is in agreement with previous studies on identical composition [29].

Figure 7 presents the power factor ($S^2\sigma$) as a function of the temperature, obtained from the values of electrical conductivity and Seebeck coefficient. As expected, the observed variations are quite similar to those displayed in Figure 5, displaying maxima at the same temperatures as the electrical conductivity (σ). The power factor for fine-size-powder derived STN5 ceramics reaches a maximum of 6.6 μW/(cm·K^2), which is more than twelve

times higher than that of the coarse-size-powder derived ceramics, and about two times higher than the value obtained by Zhang et al. with an identical composition [29], mainly due to the larger electrical conductivity of the fine-size-powder derived STN5 ceramics.
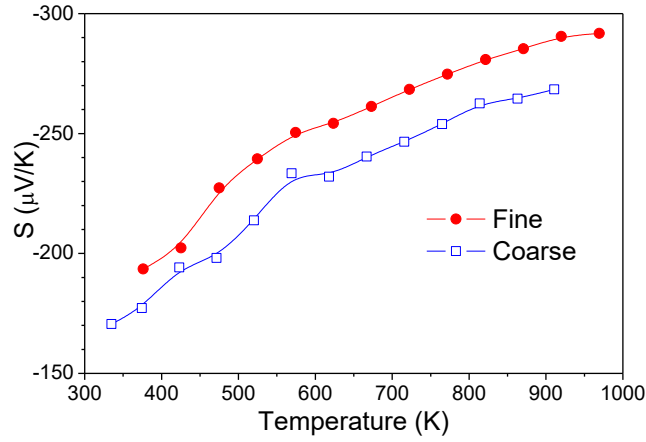

Figure 6. Seebeck coefficient *S* of STN5 ceramics produced from coarse (open squares) and fine (solid circles) particle size powders as a function of the temperature, revealing similar values for both ceramics.
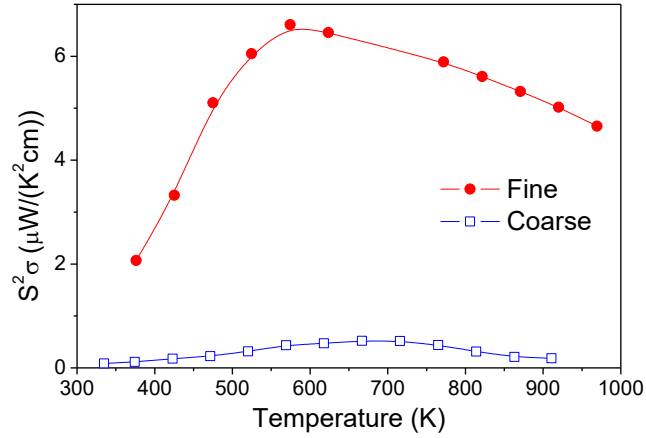

Figure 7. Power factor $S^2\sigma$ of STN5 ceramics produced from coarse (open squares) and fine (solid circles) particle size powders versus temperature, demonstrating 12 times higher values for denser fine particle size powder derived ceramics.
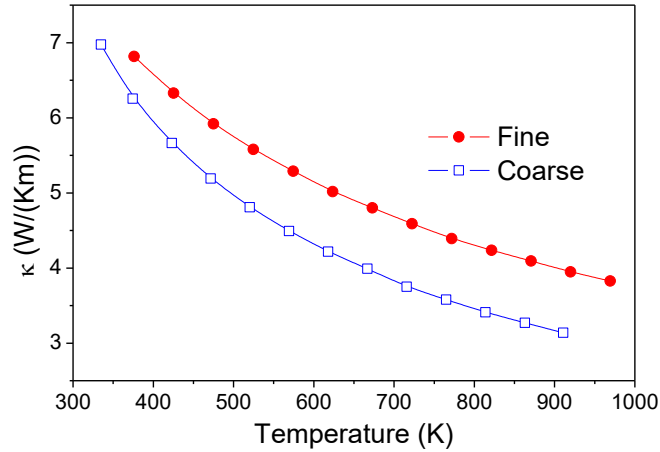
Figure 8. Thermal conductivity κ of STN5 ceramics produced from fine (solid circles) and coarse (open squares) particle size powders versus temperature, showing higher values for denser ceramics.

The thermal conductivity displays a decreasing trend with temperature for both STN5 ceramics, as seen in Figure 8. Moreover, the thermal conductivity values are smaller for the ceramics prepared from the coarse powders, probably due to higher porosity and a lower electronic thermal conductivity contribution. The lowest thermal conductivity value registered is of 3.14 W/(m·K) at 910 K.

Indeed, the thermal conductivity is known to consist of electronic and lattice components $\kappa = \kappa_e + \kappa_L$, and electronic thermal conductivity can be estimated using the Wiedemann-Franz law $\kappa_e = L{\times}T{\times}\sigma$, where L is the Lorenz number that can be deduced from the Seebeck coefficient data as $L = (1.5 + \exp[-|S|/116]){\times}10^{-8}$ V^2/K^2 [49]. Although in many studies the Lorenz number is taken as a constant $L = 2.45{\times}10^{-8}$ V^2/K^2, it is not a very precise assumption, since it approaches that value only at very low temperatures, as seen from Figure 9, which shows the Lorenz number values calculated from our Seebeck coefficient data.

From Figure 10 it is seen that the electronic thermal conductivity contribution κ_e is indeed very low for the coarse-size-powder derived STN5. For the fine-size-powder derived ceramics, it is higher but still quite low,

being below 2% of the total κ and implying that the thermal conductivity is dominated by the lattice contribution κ_L.
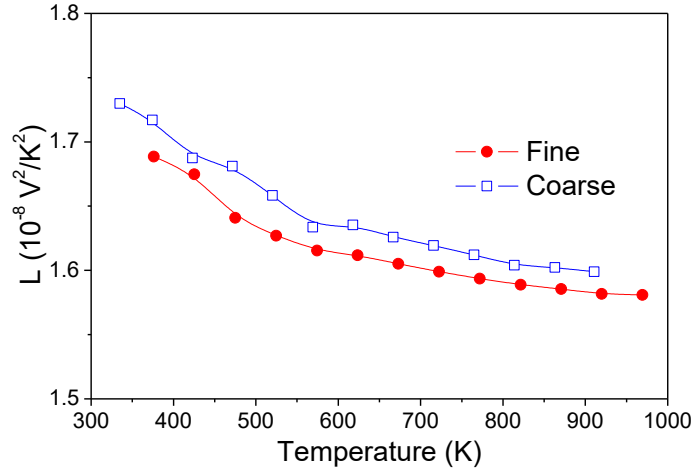

Figure 9. Temperature variation of the Lorenz number calculated from the temperature dependence of the Seebeck coefficient S in μV/K as $L = (1.5 + \exp[-|S|/116]) \times 10^{-8}$ V^2/K^2 for the ceramics produced from coarse (open squares) and fine (solid circles) particle size powders.
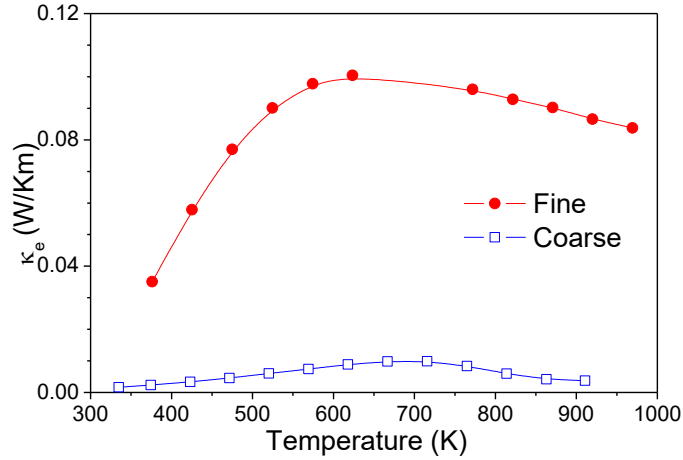

Figure 10. Electronic component of the thermal conductivity κ_e of STN5 ceramics produced from fine (solid circles) and coarse (open squares) particle size powders versus temperature, revealing a contribution below 2% to the total κ.

Finally, the figure of merit, being directly connected with the potential efficiency of the material, relates all the other TE characteristics as $ZT = S^2 \times \sigma \times T/\kappa$. For both STN5 ceramics, ZT increases with temperature as presented in Figure 11. In the case of the coarse-size-powder derived ceramics it reaches only 0.01 at 716 K, despite its reduced thermal conductivity. STN5 ceramics produced in this study from the fine particle size precursor powder reveal the highest ZT value of 0.12 at 970 K. For comparison purposes, previously reported data by Zhang et al. [29] are also shown in Figure 11. They have prepared $SrTi_{0.95}Nb_{0.05}O_{3\pm\delta}$ powders by hydrothermal methods and sintered the ceramics at 1300°C for 5 h, embedding them into carbon powder instead of using reducing atmosphere. As a result, a ZT of ~0.11 at 1000 K, increasing to ~0.37 by raising the Nb content to 10 at.%, was reported [29]. Thus, the ceramics obtained in this work by a conventional route from powder with an average particle size of 320 nm, using sintering in air at 1450ºC for 10 h and further in H_2/N_2 at 1400ºC for 10 h, possesses the highest ZT value of 0.12 at 970 K for a $SrTi_{0.95}Nb_{0.05}O_{3\pm\delta}$ composition.
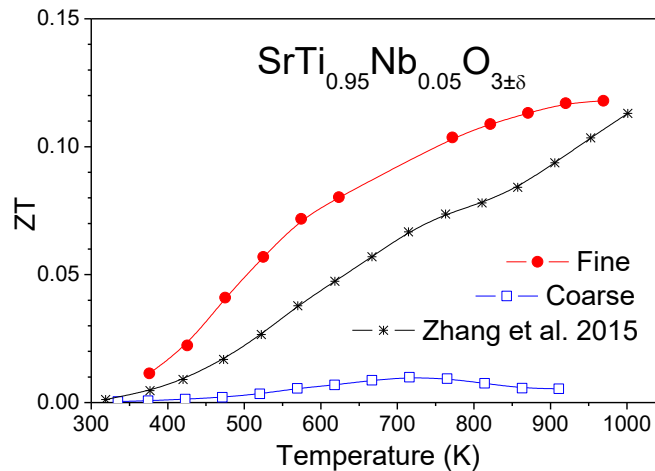

Figure 11. Dimensionless figure of merit *ZT* of STN5 ceramics produced from fine (solid circles) and coarse (open squares) particle size powders versus temperature. *ZT* data for ceramics with identical composition from Ref. 29 are shown for comparison, demonstrating that fine-size powder STN5 ceramics obtained in this work by conventional two-step sintering possess the highest *ZT* value of 0.12 at 970 K, reported up to now.

CONCLUSION

In addition to grain nano-structuring, lattice defect and grain boundary engineering approaches, with this work we have shown that the microstructure engineering of $SrTiO_3$-based ceramics by powder morphology and sintering cycle design can result in enhanced *ZT* TE *n*-type oxide ceramics. Besides the bimodal grain size distribution observed in $SrTi_{0.80}Nb_{0.20}O_{3\pm\delta}$, significant density variation in $SrTi_{0.95}Nb_{0.05}O_{3\pm\delta}$ ceramics can affect the TE performance. $SrTi_{0.95}Nb_{0.05}O_{3\pm\delta}$ ceramics produced using powders with an average particle size of ~760 nm by conventional sintering in air at 1450°C and further sintering in H_2/N_2 at 1400°C present relative density lower than 90%, and average grain size of 1.1 μm. On the other hand, those prepared from powders with a particle size of ~320 nm attain higher than 95% density and grains growing to 2.2 μm average size. The origin of such a difference is related to the fact that the densification and consequent grain growth can be achieved at lower temperature for the smaller powder particle size. As result, the *ZT* value is increased from 0.01 for conventionally prepared coarse-particle-size derived ceramics to 0.12 at 970 K for the fine-size-powder ceramics. These results on donor-doped $SrTiO_3$ ceramics contribute to enhance the performance of *n*-type oxides and to the development of high-temperature thermoelectrics for automotive and manufacturing energy-harvesting sectors.

ACKNOWLEDGEMENTS

REFERENCES

[1] Saqr, K. M., Mansour, M. K., Musa, M. N. 2008. "Thermal Design of Automobile Exhaust Based Thermoelectric Generators: Objectives and Challenges." *Int. J. Automot. Technol*. 9:155-160.

[2] Yang, J., Caillat, T. 2006. "Thermoelectric Materials for Space and Automotive Power Generation." *MRS Bull*. 31:224-229.

[3] Koumoto, K., Wang, Y., Zhang, R., Kosuga, A., Funahashi, R. 2010. "Oxide Thermoelectric Materials: A Nanostructuring Approach." *Annu. Rev. Mater. Res*. 40:363-394.

[4] Snyder, G. J., Christensen, M., Nishibori, E., Caillat, T., Iversen, B. B. 2004. "Disordered Zinc in Zn_4Sb_3 with Phonon-Glass and Electron-Crystal Thermoelectric Properties." *Nat. Mater*. 3:458-463.

[5] Venkatasubramanian, R., Siivola, E., Colpitts, T., O'Quinn, B. 2001. "Thin-Film Thermoelectric Devices with High Room-Temperature Figures of Merit." *Nature* 413:597-602.

[6] Slack, G. 1995. "New Materials and Performance Limits for Thermoelectric Cooling." In *CRC Handbook of Thermoelectrics*, edited by D. M. Rowe, 407-440. Boca Raton, USA: CRC Press.

[7] Koumoto, K., Funahashi, R., Guilmeau, E., Miyazaki, Y., Weidenkaff, A., Wang, Y. F., Wan, C. L. 2013. "Thermoelectric Ceramics for Energy Harvesting." *J. Am. Ceram. Soc*. 96:1-23.

[8] Yang, J., Stable, F. R. 2009 "Automotive Applications of Thermoelectric Materials." *J. Electron. Mater*. 38:1245-1251.

[9] Terasaki, I., Sasago, Y., Uchinokura, K. 1997. "Large Thermoelectric Power in $NaCo_2O_4$ Single Crystals." *Phys. Rev. B* 56:12685-12687.

[10] Masset, A. C., Michel, C., Maignan, A., Hervieu, M., Toulemonde, O., Studer, F., Raveau, B., Hejtmanek, J. 2000. "Misfit-Layered Cobaltite with an Anisotropic Giant Magnetoresistance: $Ca_3Co_4O_9$." *Phys. Rev. B* 62:166-175.

[11] Funahashi R., Shikano, M. 2002. "$Bi_2Sr_2Co_2O_y$ Whiskers with High Thermoelectric Figure of Merit." *Appl. Phys. Lett*. 81:1459-1461.

[12] Tkach, A., Okhay, O., Almeida, A., Vilarinho, P. M. 2017. "Giant Dielectric Permittivity and High Tunability in Y-doped $SrTiO_3$

Ceramics Tailored by Sintering Atmosphere." *Acta Mater*. 130:249-260.

[13] Tkach, A., Amaral, J. S., Amaral, V. S., Vilarinho, P. M. 2017. "Dielectric Spectroscopy and Magnetometry Investigation of Gd-doped Strontium Titanate Ceramics." *J. Eur. Ceram. Soc*. 37:2391-2397.

[14] Tkach, A., Amaral, J. S., Zlotnik, S., Amaral, V. S., Vilarinho, P. M. 2018. "Enhancement of the Dielectric Permittivity and Magnetic Properties of Dy Substituted Strontium Titanate Ceramics." *J. Eur. Ceram. Soc*. 38:605-611.

[15] Hu, Q.-G., Shen, Z.-Y., Li, Y.-M., Wang, Z.-M., Luo, W.-Q., Xie, Z.-X. 2014. "Enhanced Energy Storage Properties of Dysprosium Doped Strontium Titanate Ceramics." *Ceram. Int*. 40:2529-2534.

[16] Tkach, A., Correia, T. M., Almeida, A., Agostinho Moreira, J., Chaves, M. R., Okhay, O., Vilarinho, P. M., Gregora, I., Petzelt, J. 2011. "Role of Trivalent Sr-Substituents and Sr-Vacancies in Tetragonal and Polar States of $SrTiO_3$." *Acta Mater*. 59:5388-5397.

[17] Frederikse, H. P. R., Thurber, W. R., Hosler, W. R. 1964. "Electronic Transport in Strontium Titanate." *Phys. Rev*. 134:A442-A445.

[18] Ohta, S., Nomura, T., Ohta, H., Koumoto, K. 2005. "High-Temperature Carrier Transport and Thermoelectric Properties of Heavily La- or Nb-doped $SrTiO_3$ Single Crystals." *J. Appl. Phys*. 97:034106.

[19] Okuda, T., Nakanishi, K., Miyasaka, S., Tokura, Y. 2001. "Large Thermoelectric Response of Metallic Perovskites: $Sr_{1-x}La_xTiO_3$ ($0 < x < 0.1$)." *Phys. Rev. B* 63:113104.

[20] Ohta, S., Otha, H., Koumoto, K. 2006. "Grain Size Dependence of Thermoelectric Performance of Nb-Doped $SrTiO_3$ Polycrystals." *J. Ceram. Soc. Jpn*. 114:102-105.

[21] Kikuchi, A., Okinaka, N., Akiyama, T. 2010. "A Large Thermoelectric Figure of Merit of La-doped $SrTiO_3$ Prepared by Combustion Synthesis with Post-Spark Plasma Sintering." *Scripta Mater*. 63:407-410.

[22] Park, K., Son, J. S., Woo, S. I., Shin, K., Oh, M.-W., Park, S.-D., Hyeon, T. 2014. "Colloidal Synthesis and Thermoelectric Properties of La-doped $SrTiO_3$ Nanoparticles." *J. Mater. Chem. A* 2:4217-4224.

[23] Dehkordi, A. M., Bhattacharya, S., He, J., Alshareef, N. 2014. "Significant Enhancement in Thermoelectric Properties of Polycrystalline Pr-doped $SrTiO_3$ Ceramics Originating from Nonuniform Distribution of Pr Dopants." *Appl. Phys. Lett.* 104:193902.

[24] Dehkordi, A. M., Bhattacharya, S., Darroudi, T., Graff, J. W., Schwingenschlogl, U., Alshareef, H. N., Tritt, T. M. 2014. "Large Thermoelectric Power Factor in Pr-Doped $SrTiO_{3-\delta}$ Ceramics via Grain-Boundary-Induced Mobility Enhancement." *Chem. Mater.* 26:2478-2485.

[25] Kovalevsky, A. V., Yaremchenko, A. A., Populoh, S., Thiel, P., Fagg, D. P., Weidenkaff, A., Frade, J. R. 2014. "Towards a High Thermoelectric Performance in Rare-Earth Substituted $SrTiO_3$: Effects Provided by Strongly-Reducing Sintering Conditions." *Phys. Chem. Chem. Phys.* 16:26946-26954.

[26] Kovalevsky, A. V., Yaremchenko, A. A., Populoh, S., Weidenkaff, A., Frade, J. R. 2014. "Effect of A-Site Cation Deficiency on the Thermoelectric Performance of Donor-Substituted Strontium Titanate." *J. Phys. Chem. C* 118:4596-4606.

[27] Chen, C., Zhang, T., Donelson, R., Tan, T. T., Li, S. 2015. "Effects of Yttrium Substitution and Oxygen Deficiency on the Crystal Phase, Microstructure, and Thermoelectric Properties of $Sr_{1-1.5x}Y_xTiO_{3-\delta}$ ($0 \leq x \leq 0.15$)." *J. Alloy. Compd.* 629:49-54.

[28] Yaremchenko, A. A., Populoh, S., Patricio, S. G., Macias, J., Thiel, P., Fagg, D. P., Weidenkaff, A., Frade, J. R., Kovalevsky, A. V. 2015. "Boosting Thermoelectric Performance by Controlled Defect Chemistry Engineering in Ta-Substituted Strontium Titanate." *Chem. Mater.* 27:4995-5006.

[29] Zhang, B., Wang, J., Zou, T., Zhang, S., Yaer, X., Ding, N., Liu, C., Miao, L., Li, Y., Wu, Y. 2015. "High Thermoelectric Performance of

Nb-doped SrTiO$_3$ Bulk Materials with Different Doping Levels." *J. Mater. Chem. C* 3:11406-11411.

[30] Lu, Z., Zhang, H., Lei, W., Sinclair, D. C., Reaney, I. M. 2016. "High-Figure-of-Merit Thermoelectric La-Doped A-Site-Deficient SrTiO$_3$ Ceramics." *Chem. Mater.* 28:925-935.

[31] Kovalevsky, A. V., Aguirre, M. H., Populoh, S., Patricio, S. G., Ferreira, N. M., Mikhalev, S., Fagg, D., Weidenkaff, A., Frade, J. R. 2017. "Designing Strontium Titanate-Based Thermoelectrics: Insight into Defect Chemistry Mechanisms." *J. Matter. Chem. A* 5:3909-3922.

[32] Wang, J., Zhang, B. Y., Kang, H. J., Li, Y., Yaer, X., Li, J. F., Tan, Q., Zhang, S., Fan, G. H., Liu, C. Y., Miao, L., Nan, D., Wang, T. M., Zhao, L.-D. 2017. "Record High Thermoelectric Performance in Bulk SrTiO$_3$ via Nano-Scale Modulation Doping." *Nano Energy* 35:387-395.

[33] Tkach, A., Resende, J., Saravanan, K. V., Costa, M. E., Diaz Chao, P., Guilmeau, E., Okhay, O., Vilarinho, P. M. 2018. "Abnormal Grain Growth as a Method to Enhance the Thermoelectric Performance of Nb-doped SrTiO$_3$ Ceramics." *ACS Sustain. Chem. Eng.* 6:15988-15994.

[34] Okhay, O., Zlotnik, S., Xie, W., Orlinski, K., Hortiguela Gallo, M. J., Otero-Irurueta, G., Fernandes, A. J. S., Pawlak, D. A., Weidenkaff, A., Tkach, A. 2019. "Thermoelectric Performance of Nb-doped SrTiO$_3$ Enhanced by Reduced Graphene Oxide and Sr Deficiency Cooperation." *Carbon* 143:215-222.

[35] Lin, Y., Norman, C., Srivastava, D., Azough, F., Wang, L., Robbins, M., Simpson, K., Freer, R., Kinloch, I. A. 2015. "Thermoelectric Power Generation from Lanthanum Strontium Titanium Oxide at Room Temperature through the Addition of Graphene." *ACS Appl. Mater. Interfaces* 7:15898-15908.

[36] Okhay, O., Gonçalves, G., Dias, C., Ventura, J., Vieira, E. M. F., Gonçalves, L. M. V., Tkach, A. 2019. "Tuning Electrical and Thermoelectric Properties of Freestanding Graphene Oxide Papers by Carbon Nanotubes and Heat Treatment." *J. Alloy. Compd.* 781:196-200.

[37] Wang, N., Chen, H., He, H., Norimatsu, W., Kusunoki, M., Koumoto, K. 2013. "Enhanced Thermoelectric Performance of Nb-doped $SrTiO_3$ by Nano-inclusion with Low Thermal Conductivity." *Sci. Rep.* 3:3449.

[38] Srivastava, D., Norman, C., Azough, F., Schafer, M. C., Guilmeau, E., Freer, R. 2018. "Improving the Thermoelectric Properties of $SrTiO_3$-based Ceramics with Metallic Inclusions." *J. Alloy. Compd.* 731:723-730.

[39] Feng, X., Fan, Y., Nomura, N., Kikuchi, K., Wang, L., Jiang, W., Kawasaki, A. 2017. "Graphene Promoted Oxygen Vacancies in Perovskite for Enhanced Thermoelectric Properties." *Carbon* 112:169-176.

[40] Ohta, H., Kim, S., Mune, Y., Mizoguchi, T., Nomura, K., Ohta, S., Nomura, T., Nakanishi, Y., Ikuhara, Y., Hirano, M., Hosono, H., Koumoto, K. 2007. "Giant Thermoelectric Seebeck Coefficient of a Two-Dimensional Electron Gas in $SrTiO_3$." *Nat. Mater.* 6:129-134.

[41] Slack, G. A., Hussain, M. A. 1991. "The Maximum Possible Conversion Efficiency of Silicon-Germanium Thermoelectric Generators." *J. Appl. Phys.* 70:2694-2718.

[42] Bae, C., Park, J.-G., Kim, Y.-H. 1998. "Effect of Powder Characteristics on the Microstructure and Electrical Property of Nb-doped $SrTiO_3$." *J. Korean Phys. Soc.* 32:S296-S298.

[43] Bae, C., Park, J.-G., Kim, Y.-H. 1998. "Abnormal Grain Growth of Niobium-Doped Strontium Titanate Ceramics." *J. Am. Ceram. Soc.* 81:3005-3009.

[44] Lee, H.-Y., Kim, J.-S., Kim, D.-Y. 2000. "Fabrication of $BaTiO_3$ Single Crystals Using Secondary Abnormal Grain Growth." *J. Eur. Ceram. Soc.* 20:1595-1597.

[45] Boston, R., Schmidt, W. L., Lewin, G. D., Iyasara, A. C., Lu, Z., Zhang, H., Sinclair, D. C., Reaney, I. M. 2017. "Protocols for the Fabrication, Characterization, and Optimization of n-Type Thermoelectric Ceramic Oxides." *Chem. Mater.* 29:265-280.

[46] Alleno, E., Berardan, D., Byl, C., Candolfi, C., Daou, R., Decourt, R., Guilmeau, E., Hébert, S., et al. 2015. "Invited Article : A Round Robin Test of the Uncertainty on the Measurement of the Thermoelectric

Dimensionless Figure of Merit of $Co_{0.97}Ni_{0.03}Sb_3$." *Rev. Sci. Instrum.* 86:011301.

[47] Ning, H., Mastrorillo, G. D., Grasso, S., Du, B., Mori, T., Hu, C., Xu, Y., Simpson, K., Maizza, G., Reece, M. J. 2015. "Enhanced Thermoelectric Performance of Porous Magnesium Tin Silicide Prepared Using Pressure-less Spark Plasma Sintering." *J. Mater. Chem. A* 3:17426-17432.

[48] Li, E., Wang, N., He, H., Chen, H. 2016. "Improved Thermoelectric Performances of $SrTiO_3$ Ceramic Doped with Nb by Surface Modification of Nanosized Titania." *Nanoscale Res. Lett*. 11:188.

[49] Kim, H. S., Gibbs, Z. M., Tang, Y., Wang, H., Snyder, G. J. 2015. "Characterization of Lorenz Number with Seebeck Coefficient Measurement." *APL Mater.* 3:041506.